ACS APPLIED NANO MATERIALS

Open Access

This article is licensed under CC-BY 4.0

www.acsanm.org

Article

Effect of Cerium Precursors on Ce-Doped $BiVO_4$ Nanoscale-Thick Films as Photoanodes: Implications for Water Splitting

Matheus G. Guardiano, Lara K. Ribeiro, Isabelle M. D. Gonzaga, and Lucia H. Mascaro*

Cite This: *ACS Appl. Nano Mater.* 2024, 7, 19569−19578

Read Online

ACCESS | Metrics & More | Article Recommendations | Supporting Information

ABSTRACT: The use of the $BiVO_4$ semiconductor to generate H_2 via water splitting has recently been studied to meet the global energy demand. However, $BiVO_4$ has some limitations such as higher electron−hole recombination and poor stability, being necessary studies that aim to give better performance. In this scenario, the use of the rare earths as a doping agent should be considered. This work explores the nanoscale-thick film $BiVO_4$ electrochemical synthesis via BiOI film obtention and the effects of the use of different cerium precursors on the physical and photoelectrochemical (PEC) properties. Cerium(III) nitrate, cerium(IV) oxide, and ammonium cerium(IV) nitrate were evaluated as precursors and added into the plating solution before the electrochemical deposition. The films obtained underwent characterization through X-ray diffraction, SEM-EDS, and micro-Raman analyses. The results indicate that cerium is incorporated into the $BiVO_4$ structure and that this incorporation did not alter its monoclinic structure, confirming the successful execution of the doping process. The PEC film characterization was evaluated by cyclic voltammetry, linear sweep voltammetry, and electrochemical impedance spectroscopy, showing a different PEC activity that depends on the used cerium precursors. The use of ammonium cerium(IV) nitrate improves the activity of the Ce−$BiVO_4$ films, increasing the photocurrent by almost 2 times compared with pure $BiVO_4$. Otherwise, the other precursors decrease the activity. Analysis of the ultraviolet−visible reflectance spectra and Mott−Schottky plots showed the difference between the material band gap and conduction band, highlighting that the use of different cerium precursors must be carefully evaluated to obtain a Ce−$BiVO_4$ film with a lower electron−hole recombination. These achievements highlight the importance of understanding the effect of a cerium precursor on nanoscale-thick Ce-doped $BiVO_4$ obtention for water-splitting applications as a photoanode.

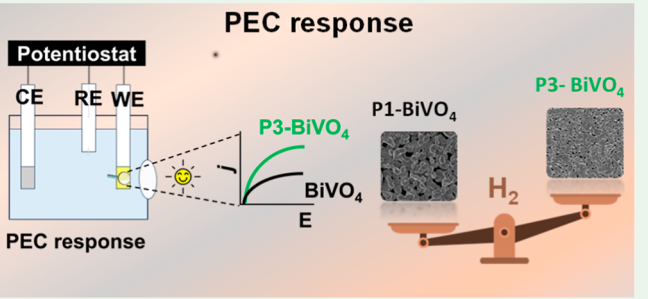

KEYWORDS: *water splitting, cerium precursors, photoanode, doping, H_2 generation*

Downloaded via UNIV FED DE SAO CARLOS on September 6, 2024 at 17:09:33 (UTC).
See https://pubs.acs.org/sharingguidelines for options on how to legitimately share published articles.

INTRODUCTION

One of the biggest global scientific challenges currently expanding is seeking solutions to meet global energy demand.[1] As an example of economic measures, the European Union invested 2 billion euros in the production of green hydrogen in Brazil, as part of the European bloc's plans to reduce dependence on and use of fossil fuels.[2] The production of H_2 stands out as a viable renewable energy source, which can be realized through different processes, such as photocatalysis or photoelectrocatalysis.[3] The objective to meet the global demand is to expand the production of green hydrogen by integrating different approaches to obtain it. In this scenario, the development of semiconductors capable of generating O_2 and H_2 via water splitting stands out.[4]

A promising semiconductor for photoelectrocatalytic applications is bismuth vanadate ($BiVO_4$).[5] It has a band gap close to 2.4 eV and activity when irradiated with solar radiation, making it interesting to evaluate its application for water splitting and oxidation of different organic contaminants.[6−10] However, $BiVO_4$, like other semiconductors that have a band gap in the visible region, has a high recombination rate and low stability, thus requiring designer efforts of new materials to optimize stability and reduce electron−hole pair recombination before their efficient application as an photoanode. Among the possibilities for optimizing the material, doping of cations, such as rare earth metals, is promising. These elements have unique properties, such as unique electronic arrangement characteristics, large ionic radius, and strong metal activity which make them highly attractive in several lines of research, including catalysis and materials science.[11] It can lead to the ion's replacement in the material's crystalline structure and create intermediate energy levels between the valence band (VB) and conduction band (CB). It

Received: June 20, 2024
Revised: August 6, 2024
Accepted: August 8, 2024
Published: August 14, 2024

© 2024 The Authors. Published by American Chemical Society

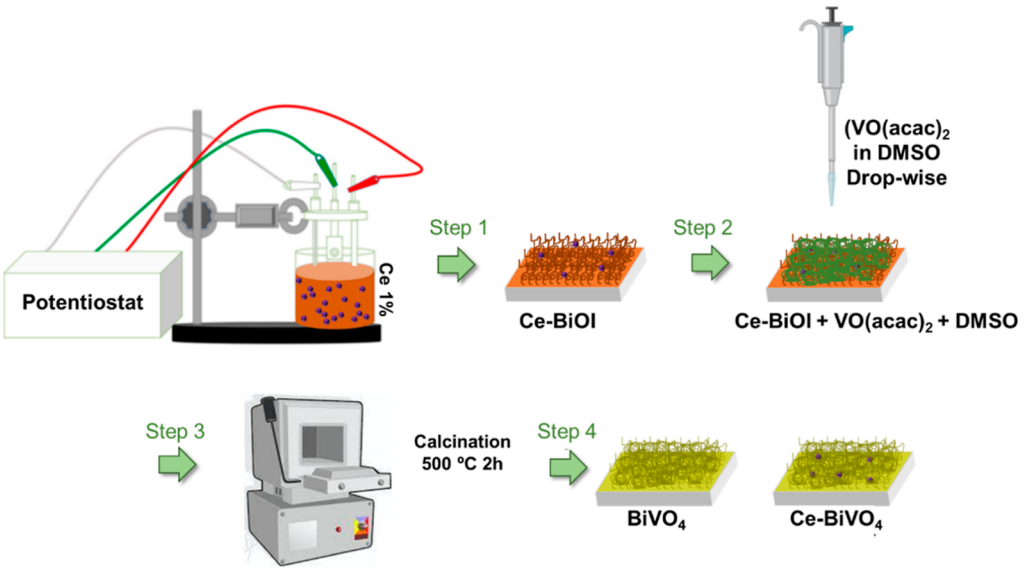

Figure 1. Schematic diagram of the synthesis of $BiVO_4$ and Ce−$BiVO_4$ by the electrodeposition method.

can cause a reduction in recombination and provide stability to the material,[12] resulting in a better nanoscale photoanode performance for water splitting.

Govindaraju et al.[13] investigated doping at the Bi^{3+} site through the addition of lanthanide elements, seeking to understand how rare earths influence the electronic band structure of $BiVO_4$. They doped $BiVO_4$ with La^{3+}, Ce^{3+}, Sm^{3+}, and Yb^{3+}. The results obtained demonstrated that modifications with rare earths in the $BiVO_4$ structure can cause changes in the electronic band structure, which can be associated with the formation of oxygen vacancies, which, when combined, are considered more efficient for the application of water separation in relation to a pure material. Tian et al.[14] were the pioneers in doping Nd^{3+} into the $BiVO_4$ structure, aiming at photoelectrochemical (PEC) studies for water separation. The researchers employed a cocatalyst ($NiFe_2O_4$) to further improve the PEC system. The photocurrent density of the synthesized $NiFe_2O_4$−Nd−$BiVO_4$ photoanode reaches 1.93 mA cm^{-2} at 1.23 V versus RHE, which is 3 times higher than that of the reported pure $BiVO_4$ photoanode.

Following this approach, Wang et al.[15] explored the doping of Nd^{3+} and CoOOH (cocatalyst) to improve the efficiency of $BiVO_4$. The CoOOH−Nd−$BiVO_4$ photoanode exhibits an impressive photocurrent density of 2.4 mA cm^{-2} at 1.23 V versus RHE, which is 2.67 times higher than that of pure $BiVO_4$. Their results indicated that the insertion of Nd^{3+} resulted in improvements in the material's photocurrent, in addition to providing greater stability to $BiVO_4$. Based on the results obtained by Govindaraju et al.,[13] Tian et al.,[14] and Wang et al.,[15] it is possible to bet on the possibilities of optimizing $BiVO_4$ through the doping of cations, such as rare earth metals. The use of rare earths can lead to the replacement of the ion in the crystalline structure of the material, being Bi^{3+} and/or V^{5+}, and create intermediate energy levels between the VB and CB. Furthermore, they can cause a reduction in recombination and provide an improvement in the stability of the material. These insights reveal that studies to improve the effect of doping are necessary.

To enhance the doping effect, many studies are currently focusing on the influence of concentration and variety of rare earths on the crystal structure of $BiVO_4$.[16−18] To date, there is no research on the effects of rare earth precursor sources on the structure of $BiVO_4$. In addition, Chen et al.[19] investigated the impact of different cerium precursors (cerium chloride and cerium nitrate) on the properties of ZnO deposited on *p*-GaN and ITO substrates. The two cerium precursors resulted in distinct current−voltage curves as well as discrepant electroluminescence and photoluminescence spectra. The relative contributions of green and orange-red emissions to the emission spectra of the annealed samples also depended on the precursor used. This indicates that the types and concentrations of native defects varied depending on the precursor used. This study shows that even a specific precursor source can contribute to the optimization of rare earth doping in systems, aiming for a more efficient application. Therefore, it is necessary to investigate the sources of precursors in the synthesis of rare earth doping in structured $BiVO_4$ and explore the potential for its application in practical devices.

The influence of the concentration of the rare earth element Ce^{3+}[13] and other rare earths has already been studied.[14,15,18,20] However, the effect of using Ce^{3+} precursors other than the commonly used cerium nitrate has not yet been investigated in electrochemical studies and is an important factor that can affect the $BiVO_4$ photoanode stability. Therefore, we explored the impact of different Ce^{3+} precursors on the properties of nanoscale-thick Ce-doped $BiVO_4$ photoanodes and characterized the films obtained in order to understand the influence of cerium on the physical and PEC semiconductor properties for water splitting.

MATERIALS AND METHODS

Chemicals. Cerium(IV) oxide (99.9%, Sigma-Aldrich), cerium(III) nitrate (Alfa Aesar, 99.5%), and ammonium cerium(IV) nitrate (VETEC, 99%) were used as cerium precursors, named P1, P2, and P3, respectively. $Bi(NO_3)_3$ (≥98%), isopropanol (99.8%), and vanadium(III) acetylacetonate (97%) were purchased from Sigma-Aldrich. KI (≥99.0%) and HNO_3 (65%) were acquired from Neon. Ethanol (Dinâmica, ≥99.5%), *p*-benzoquinone (Alfa Aesar, ≥98%), H_2O_2 (Êxodo, 30% (v/v)), acetone (Qhemis, 99.5%), Na_2SO_4 (Synth, 99.0%), and DMSO (Supelco, 99.5%) were also used.

Catalyst Synthesis and Physical Characterization. $BiVO_4$ films were produced by electrodeposition as reported before.[21] A solution containing 50 mL of KI 0.4 mol L^{-1} and Bi^{3+} 0.04 mol L^{-1}

https://doi.org/10.1021/acsanm.4c03537
ACS Appl. Nano Mater. 2024, 7, 19569−19578

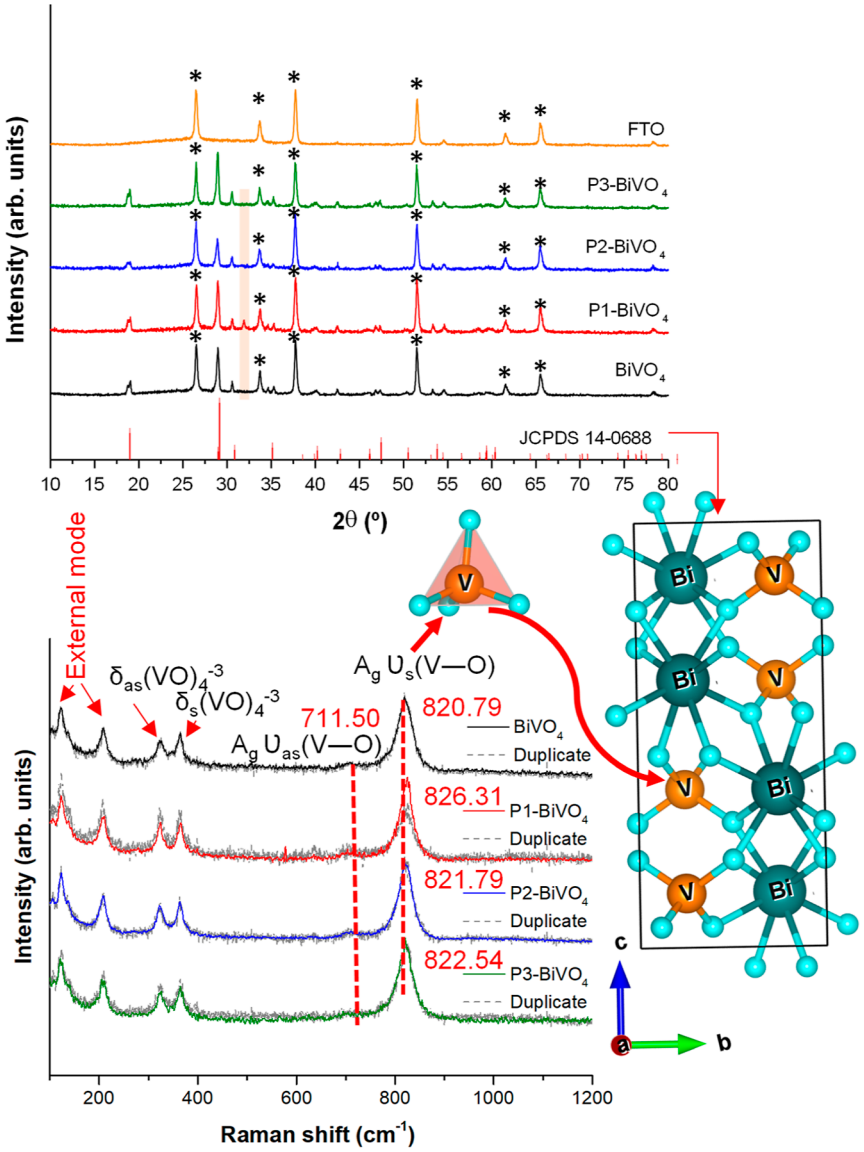

Figure 2. (a) XRD patterns of $BiVO_4$ and Ce−$BiVO_4$ samples using various precursors. The red lines represent the indexed space group (ISCD) for the monoclinic structure with reference number 62706. (b) Raman spectra for both $BiVO_4$ and Ce−$BiVO_4$ samples.

was prepared using Milli-Q water and the pH was adjusted to 1.7 with HNO_3. Another solution of 0.23 mol L^{-1} *p*-benzoquinone was prepared in ethanol and mixed with the solution with pH adjustment. $Ce(NO_3)_3$, $(NH_4)_2Ce(NO_3)_6$, and CeO_2 (after the reaction with HNO_3, further enhancement is achieved with the assistance of H_2O_2) were added into the different prepared Bi^{3+} solutions before pH adjustment at a concentration of 1% of cerium for the Ce−$BiVO_4$-doped film production, named as P1−$BiVO_4$, P2−$BiVO_4$, and P3−$BiVO_4$, respectively. These plating solutions were stored at 4 °C for a maximum of 1 month.

The $BiVO_4$ and Ce−$BiVO_4$ films were produced at 4 different steps (Figure 1). The first one consisted of BiOI film electrodeposition in a three-electrode cell using FTO as the WE (previously cleaned using acetone, ethanol, isopropanol, and water), graphite as the counter electrode, and Ag/AgCl/saturated KCl (Ag/AgCl) as the reference. The BiOI film electrodeposition was performed at room temperature applying −0.1 V vs Ag/AgCl limited with a deposition charge of −0.1 C cm^{-2}. The second step consists of dropwise addition of 50 mL of vanadium(III) acetylacetonate [$VO(acac)_2$] 0.2 mol L^{-1} in DMSO solution. Finally, the electrodes were calcined at 500 °C for 2 h (step 3) and washed for 30 min using NaOH 1 mol L^{-1} (step 4) for vanadium excess removal after thermal treatment.

The phase compositions of the samples were characterized by X-ray diffraction (XRD, Shimadzu 6000 XRD Protocol). Measurements of micro-Raman were performed by the iHR550 spectrometer (Horiba Jobin-Yvon) coupled to a silicon CCD and an ion laser (Melles Griot, 614 nm, 200 mW). The morphology of the films was characterized by scanning electron microscopy−energy-dispersive spectroscopy (SEM-EDS; TM4000 Plus, Hitachi), operating at 15 kV, and field-emission scanning electron microscopy (FE-SEM, Jeol JSM-7200F). The investigation of the optical properties of the samples was performed by ultraviolet−visible (UV−vis) spectroscopy. The value of optical energy band gap (E_{gap}) was calculated using the Kubelka and Munk−Aussig method from UV−vis diffuse reflectance measurements that were performed using a Varian Cary spectrometer model 5G in the diffuse reflectance mode, with a wavelength range of 300 to 800 nm and a scan speed of 600 nm min^{-1}.

PEC Analysis. PEC analysis was performed in a three-electrode cell filled with 0.5 mol L^{-1} Na_2SO_4 solution (pH 7.0) using $BiVO_4$ and Ce−$BiVO_4$ as the WE, platinum as the counter electrode, and Ag/AgCl as the reference. The Nernst equation (eq 1) was used to convert the Ag/AgCl electrode potential to RHE, where E_{RHE} is the potential versus RHE, $E^{\circ}_{Ag/AgCl}$ is 0.197 V at 25 °C, $E_{Ag/AgCl}$ is the

https://doi.org/10.1021/acsanm.4c03537
ACS Appl. Nano Mater. 2024, 7, 19569−19578

potential versus Ag/AgCl measured, and pH is 7.0. All measurements were carried out at room temperature and in triplicate.

$$E_{RHE} = E_{Ag/AgCl} + E^{\circ}_{Ag/AgCl} + (0.059 \times pH) \quad (1)$$

The PEC measurements were carried out using a potentiostat/galvanostat (PGSTAT302N, Autolab, Metrohm). The light source was a sunlight simulator (Oriel, LCS-100) with 100 mW cm^{-2} of irradiance and the WE exposed area was 1 cm^2 from the back side. The cyclic voltammetry (CV) curves were obtained in three cycles ranging from −0.4 to 2.3 V vs RHE at 10 mV s^{-1}. Dark/light linear sweep voltammetry (LSV) staircase curves were obtained at a 5 mV s^{-1} scan rate. Electrochemical impedance spectroscopy (EIS) was performed at 1.05 V vs RHE (on-set potential) in the dark and under irradiation with 10 mV amplitude in the frequency range from 10 kHz to 10 Hz. The M−S measurement was performed by measuring the impedance spectra of the samples over a potential range of −0.4 to 2.3 V vs RHE, with a potential step of −0.02 V at 100 Hz.

RESULTS AND DISCUSSION

Physical Characterization. The XRD patterns of all as-prepared $BiVO_4$ and Ce−$BiVO_4$ are shown in Figure 2a. It can be seen that the $BiVO_4$ film has a monoclinic structure; from the XRD patterns, it is visible that the 2θ values 19, 28, 31, 30, and 46° matched completely with the scheelite-type monoclinic $BiVO_4$ phase (standard card JCPDS. no. 14-0688; space group: $I2/a$, a = 5.195, b = 11.701, c = 5.092, β = 90.38°).[22,23] The diffraction peaks at 26, 33, 37, 51, 61, and 65° belong to the SnO_2 in FTO glass (JCPDS. no. 41-1445)[24] used for electrodeposition of the material. An additional phase is identified in the P1−$BiVO_4$ material following doping with Ce^{3+} ions, as evidenced by a peak at around 32.5°, indicating the presence of CeO_2 (JCPDS. no. 01-081-0792).[25] Additionally, there exists the potential for the formation of CeO_2 on the material's surface; this formation originates from CeO_2 as its precursor. However, regarding precursors P2 and P3, this implies that the introduction of Ce^{3+} does not prompt structural alterations in $BiVO_4$, as evidenced by the absence of a peak in the 32.5° region. Similar results were found in the literature when studying the efficient percentage for doping $BiVO_4$ with cerium.[11,26] In these studies, when doping was carried out (regardless of the percentage of cerium), no changes were found in the monoclinic phase of $BiVO_4$. The authors concluded that it was an indication of doping, since the replacement of Bi^{3+} by doped cerium ions is possible, since the ionic radius of Bi^{3+}, Ce^{3+}, and Ce^{4+} is 1.17, 1.14, and 1.01 Å, respectively.[11,26] Remarkably, there are no observable shifts in the highest-intensity peaks of $BiVO_4$, signifying that the low concentration of Ce^{3+} ions has minimal impact on the atomic positions within the crystalline structure of $BiVO_4$.

The Raman spectra of $BiVO_4$ and Ce−$BiVO_4$ powders were excited by a red (633 nm) laser and the corresponding spectra are shown in Figure 2b. The Raman bands around at 121, 208, 320, 364, 711, and 820 cm^{-1} were detected in all samples.[27] The bands centered at 320 and 364 cm^{-1} delineate the asymmetric and symmetric configurations of the [VO_4] tetrahedron, respectively. The stretching modes of two distinct types of V−O bonds are discerned through bands centered at 711 and 820 cm^{-1}.[28,29] These spectral features furnish valuable insights into the structural divergences between film samples subjected to electrodeposition with different Ce^{3+} precursors. An observable positive shift in the vibrational mode of V−O was noted, with recorded values of 819.03, 825.30, 820.70, and 823.55 cm^{-1} for $BiVO_4$, P1, P2, and P3, respectively. This variation potentially correlates with alterations in the length of the V−O bond, suggesting changes within the $BiVO_4$ unit cell induced by the incorporation of Ce^{3+}.[30−32] While the specific sites of Ce^{3+} exchange (V^{5+} or B^{3+}) remain uncertain, these subtle alterations signify an ongoing doping process within the bulk of the material.

The surface morphologies of the prepared materials, visualized using SEM images, are shown in Figure 3a−d, and

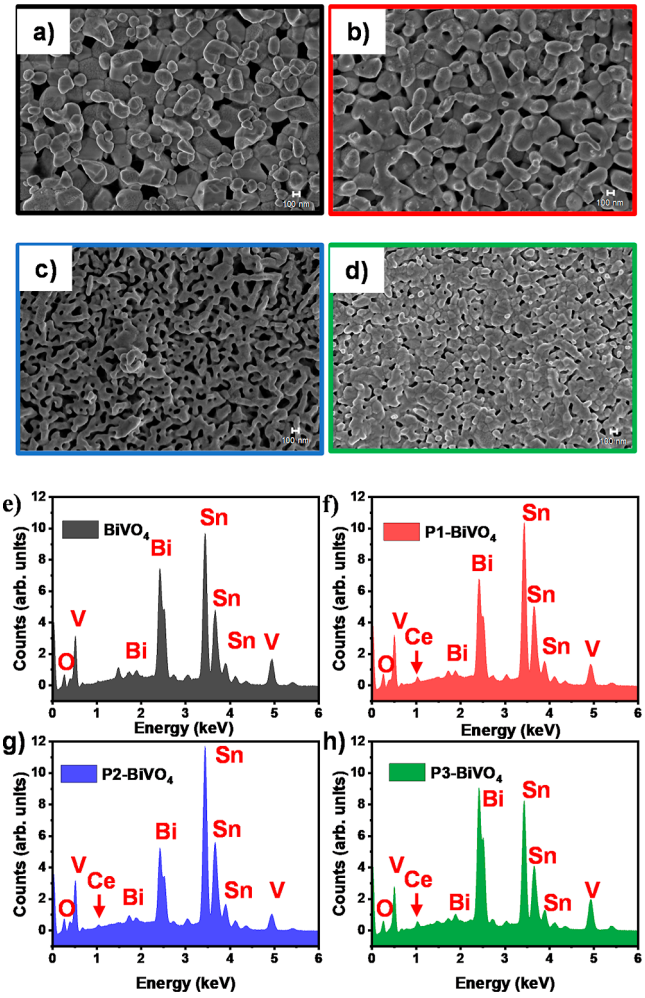

Figure 3. SEM-EDS spectra analysis conducted on various surfaces: $BiVO_4$ (a,e), Ce−$BiVO_4$: P1 (b,f), P2 (c,g), and P3 (d,h).

it was observed that the thickness of all films is around 520 nm. The images highlight how $BiVO_4$ particles form clusters in the FTO glass, exhibiting irregularities. Electrodeposition of pure $BiVO_4$ revealed the greatest variation in FTO, evidenced by cracks along the perimeter of the film in the SEM images (SEM images with low magnification can be observed at Figure S1). Intriguingly, samples synthesized with P1, P2, and P3 show a more uniform distribution of $BiVO_4$ throughout the FTO. In addition to uniformity, it is observed that samples P1 and P2 exhibit gaps between the FTO and the particles, while the opposite is evident in P3, which presents a greater coverage of particles across the entire surface of the FTO. A greater FTO coverage can improve semiconductor photocurrent response due to the enhanced light absorption and increased surface area for PEC water oxidation on the surface.[33,34]

To ascertain the presence of Ce^{3+} in $BiVO_4$, EDS analysis was conducted on the $BiVO_4$ and Ce−$BiVO_4$ samples. It was

https://doi.org/10.1021/acsanm.4c03537
ACS Appl. Nano Mater. 2024, 7, 19569−19578

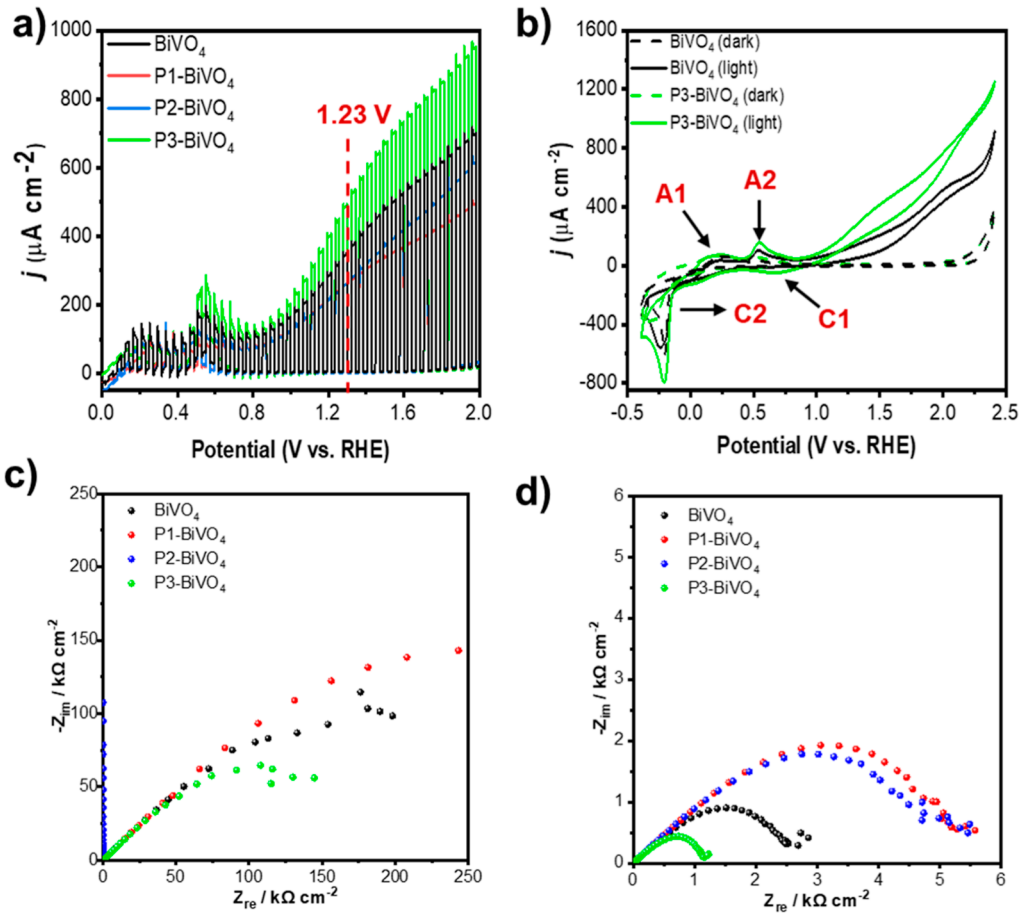

Figure 4. (a) Linear voltammograms under intermittent illumination at a 5 mV s^{-1} scan rate; (b) cyclic voltammograms at a 10 mV s^{-1} scan rate in the dark and light (third cycle); and Nyquist EIS plots in the (c) dark and (d) simulated sunlight exposure. All the experiments were done in 0.5 mol L^{-1} Na_2SO_4 solution pH 7.

observed that, in addition to Bi, V, O, and I, Ce was also present in the samples (P1, P2, and P3) without other impurities (Figure 3e–h).[35] However, the percentage of Ce 1% in the bulk material is low compared to the other elements, and its actual concentration in the sample cannot be disclosed because the Ce Kα peak overlaps with the V Kα peak at approximately 4.98 keV. Nevertheless, the presence of Ce^{3+} can be inferred through the appearance of the Ce Mα peak at around 0.98 keV. This indication reveals the occurrence of doping in the $BiVO_4$ structures synthesized with different cerium precursors. In addition, using the Ce Mα peak, it can be inferred that the cerium content is less than 0.7% for all samples. It highlights that the use of different precursors implies in different FTO coverage and consequently cerium content.

PEC Characterization. It was studied how the electrodeposition time interferes with the electrodeposited charge on the FTO substrate surface (Figure 4). It was observed that the electrodeposited charges applying a fixed potential (−0.1 V vs Ag/AgCl) in the same time interval for pure $BiVO_4$ solution (P) and doped with different cerium precursors (P1, P2, and P3) vary between materials. This result indicates that the addition of precursors to the electrodeposition solutions possibly changed some property, such as ionic strength, due to the fact of using different cerium salts in different oxidation states (Ce^{3+} or Ce^{4+}). The PEC characterizations of these electrodeposited films at different time intervals can be consulted in the Supporting Information (Figures S2 and S3). In view of the preliminary results observed by electrodeposited films at different time intervals, it was decided to standardize the electrodeposited Ce–BiOI charge to −0.1 C (Figure S4). This standardization was important to seek a better comparison between the films and guarantee a lower error associated with the results obtained in the PEC characterization.

PEC characterizations were carried out to verify the influence of different cerium precursors on the properties of Ce–$BiVO_4$ films obtained after heat treatment. Photocurrent and EIS measurements (Figure 4) show that the use of different precursors affected the properties of the films, indicating that the cerium ions present in the electrodeposition solution were inserted into the structure of the obtained films. Cerium ions were inserted into the BiOI structure by a carried that occurred during the bismuth electrodeposition in the benzoquinone oxidation process on the FTO substrate surface.[21] At this scenario, on the FTO surface remain BiOI and cerium, which during thermal conversion to $BiVO_4$ implies into Bi replacements for Ce.

The value of photocurrent density (j_{pc}) at 1.23 V vs RHE (water oxidation potential) for the pure $BiVO_4$ film is 286 μA cm^{-2}, while for doping using precursors P1, P2, and P3 it is, respectively, 218, 219, and 398 μA cm^{-2}. These measurements demonstrate that P3 considerably improved the photoanode activity compared to the pure $BiVO_4$ film, which was not

https://doi.org/10.1021/acsanm.4c03537
ACS Appl. Nano Mater. 2024, 7, 19569−19578

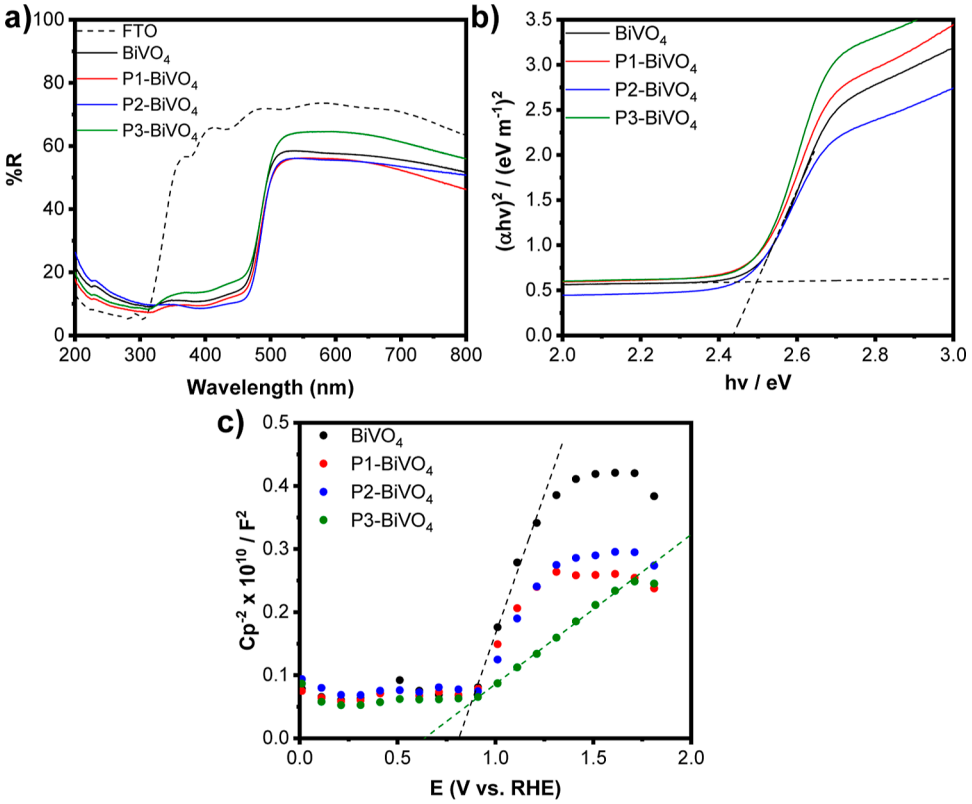

Figure 5. (a) UV−vis diffuse reflectance spectra of $BiVO_4$ and Ce−$BiVO_4$; (b) Kubelka and Munk−Aussig plot; (c) M−S plot for the obtained photoanodes (100 Hz).

observed when using P1 and P2. It is worth noting that the j_{pc} values were obtained from the difference in photoanode current in the dark and in the presence of light.

These results indicate that the use of free cerium ions in solution (P1 and P2) did not favor the increase in j_{pc}, while the use of cerium and ammonium nitrate (P3) increased this property (Figure 4a). This may occur due to the deposition process of BiOI films, which cannot be totally uniform. In this case, the presence of ammonium with cerium may have facilitated the insertion of Ce^{3+} into the BiOI film structure and changed the j_{pc} measured values. Furthermore, although different cerium precursors with different oxidation states (Ce^{3+} and Ce^{4+}) are used, at pH 1.7, the predominant cerium species is Ce^{3+}. Other authors who investigated the electrodeposition of different cerium precursors on the ZnO nanorod structure also found that not all precursors increased the current measured at the same potential value for the evaluated doping.[19]

Although the precursors P1 and P2 are different, during the procedure of CeO_2 opening with HNO_3 and H_2O_2, a solution containing Ce^{4+} and nitrate ions was formed. This procedure is important because it is not possible to use cerium in the oxide form. With the pH adjustment, the P1 solution started to show the presence of Ce^{3+}. Therefore, the electrodeposited solutions containing P1 and P2 consist of almost the same composition, and the results obtained were close.

The results indicate that P3 use improves the $BiVO_4$ anodic photocurrent. Other works in the literature have verified that doping with other rare earths also improves the j_{pc}.[14,36−38] It was reported that $BiVO_4$ doping with neodymium (Nd) improves j_{pc} because its insertion into the $BiVO_4$ crystal structure induces a lattice distortion that increases the light absorption capacity and generates more photogenerated carriers.[14] In addition, the Nd empty 4f orbital can decrease electron−hole pair recombination by developing a spatial electric field that consequently improves the j_{pc}.

CV was employed to investigate the oxidation and reduction peaks of the obtained materials (Figure 4b). Experiments using $BiVO_4$ and P3−$BiVO_4$ were done in the dark and in the presence of light, which resulted in the appearance of two oxidation peaks (A1 and A2) and two reduction peaks (C1 and C2) for P3−$BiVO_4$ under simulated sun light exposure. For $BiVO_4$, the reduction peak C1 was not observed (Figure 4b).

The anodic peak A1 (0.2 V vs RHE) is assigned to Bi^0 oxidation to Bi^+, while the peak A2 (0.55 V vs RHE) is assigned to Bi^+ oxidation to Bi^{3+}. Otherwise, the cathodic peak C2 (−0.2 V vs RHE) is associated with Bi^{3+} reduction to Bi^0.[39] The cerium insertion into the P3−$BiVO_4$ structure did not affect the electrochemical response of the obtained material in the investigated potential window. In addition, the appearance of a cathodic peak C1 (0.7 V vs RHE) in the presence of light indicates the Ce^{4+} reduction to Ce^{3+}.[40] Those results combined with the physical characterization corroborate the cerium insertion into the P3−$BiVO_4$ structure.

EIS was employed to obtain information about charge transfer processes at the synthesized photoanode interface (Figure 4b,c). According to ref 41, a smaller semicircle arc in the Nyquist plot is related to lower resistance to electron transfer and an effective separation of photogenerated electron−hole pairs. Experiments were carried out in the absence and presence of light and the processes that occur at the semiconductor interface were interpreted in terms of equivalent circuit models.[42] A greater dispersion is observed in the Nyquist plots in experiments carried out in the dark, with a

https://doi.org/10.1021/acsanm.4c03537
ACS Appl. Nano Mater. 2024, 7, 19569−19578

decrease in the resistivity of P3−$BiVO_4$ compared to $BiVO_4$. Meanwhile, the use of P1−$BiVO_4$ slightly increased the resistivity of the semiconductor but with a resistivity close to that of the undoped semiconductor. This was not observed for P2−$BiVO_4$, which had a high resistivity, and it was not possible to observe the formation of an arc in the dark. Furthermore, it is possible to evaluate the impedance spectra of all materials under simulated solar irradiation, where the arcs are clearly smaller than those obtained in the dark. This behavior is attributed to the photogenerated current, which results in a decrease in resistance to charge transfer.[43,44]

In experiments carried out in the presence of light, two semiarc formations for each curve are observed. In this case, doping with P3−$BiVO_4$ considerably reduced the resistivity of the semiconductor. Meanwhile, doping using P1−$BiVO_4$ and P2−$BiVO_4$ increased the resistivity of the semiconductor compared to that of pure $BiVO_4$. This indicates that the charge transfer process is not favored when P1 and P2 were used. Similarly, the clear results obtained in the EIS for the P1 and P2 precursors were very close, similar to what was discussed in the j_{pc} analyses.

It is observed that P3−$BiVO_4$ can accelerate charge transfer processes between the electrolyte and the semiconductor interface by suppressing electron−hole pair recombination. The obtained results combined with stability tests (Figure S5) demonstrated a better performance of the P3−$BiVO_4$ photoanode for water splitting. In a study that evaluated the different atoms' doping in the $BiVO_4$ structure, it was found that the doping of Mo and W also decreased the resistivity of $BiVO_4$, facilitating the transport of electrons from the CB to the contact and from the holes in the VB for the electrolyte.[45]

A study was carried out to understand how doping with different cerium precursors affects the band gap values and the CB and VB position of semiconductors. Reflectance analysis in the UV−vis region was used to determine the photoanode band gap (Figure 5a,b). The CB and VB values for each semiconductor were obtained indirectly by using the M−S plot (Figure 5c).

The band gap values were obtained by the Kubelka and Munk−Aussig plot (Figure 5b), all of which are presented in Table 1. $BiVO_4$ presented a band gap value equal to 2.49 eV, close to that reported in the literature. Doping with P1−$BiVO_4$ and P2−$BiVO_4$ had little influence on the band gap values, presenting values of 2.47 and 2.48 eV, respectively, values that are within the standard deviation of ±0.02 eV. Cerium doping in the P3−$BiVO_4$ photoanode decreases the band gap value to 2.44 eV. This value justifies a lower recombination of electron−hole pairs observed for P3−$BiVO_4$ based on the interpretation of EIS data, which implies a higher j_{pc} due to the intermediate energy states that cerium can provide when inserted into the structure of the $BiVO_4$. In this case, the use of the P3 precursor showed better performance to improve the photocatalytic activity of $BiVO_4$ compared with other precursors.

Table 1. Parameters of M−S and Band Gap Analyses of Different $BiVO_4$ Films Doped with Cerium

parameters	$BiVO_4$	P1−$BiVO_4$	P2−$BiVO_4$	P3−$BiVO_4$
E_{fb} (V vs RHE)	0.84	0.80	0.87	0.64
E_g (eV)	2.49	2.47	2.48	2.44
E_{CB} (V vs RHE)	0.84	0.80	0.87	0.64
E_{VB} (V vs RHE)	3.33	3.27	3.35	3.08

The M−S plot can be used to determine the flat band value (E_{fb}) and the semiconductor type (p or n).[46] The E_{fb} in the M−S plot comes from the extrapolation of the $1/C_{SC}^2 = 0$ curve on the potential axis, with C_{SC} being the capacitance of the semiconductor−electrolyte junction measured during the analysis. The type of semiconductor is estimated from the slope of the curve used to determine E_{fb}, being an n-type semiconductor when the slope is positive and a p-type when the slope is negative.[47] Furthermore, in the case of n-type semiconductors, the E_{fb} obtained in the M−S plot is close to the E_{CB} potential value, and E_{VB} can be determined indirectly ($E_{VB} = E_{CB} + E_g$).

The values of E_{fb}, E_{CB}, E_{VB}, and the semiconductors type are also presented in Table 1. It is observed that the E_{fb} for $BiVO_4$ is 0.84 V vs RHE and for a shift in E_{fb} to negative potentials when doping with P1 and P3, 0.80 and 0.64 V vs RHE, respectively. In the case of P2−$BiVO_4$, doping moved the potential to a more positive potential region (0.87 V vs RHE). The 200 mV shift between P3−$BiVO_4$ and $BiVO_4$ indicates that doping affected the E_{fb} and consequently modified the photoanode structure, decreasing the E_{CB} and E_{VB} value. This change implies a greater activity of P3−$BiVO_4$ in a smaller potential region, expanding its application as a semiconductor. Both materials present activity for the water oxidation reaction, which occurs at 1.23 V vs RHE.

Cerium insertion into the $BiVO_4$ structure was also investigated by other authors. The use of cerium nitrate as a precursor in a nonaqueous synthesis led to a better performance of Ce−$BiVO_4$.[48] In a study that used $(NH_4)_2Ce(NO_3)_6$ as a precursor in a impregnation synthesis method in aqueous solution,[26] it was observed that cerium was successfully inserted into the $BiVO_4$ structure, increased the photocurrent from 2 to 4 mA cm^{-2}, and decreased the semiconductor resistivity. These results combined with the discussed results in this work showed that not only the use of different precursors but also the synthesis method influenced the Ce−$BiVO_4$ material formation and its PEC activity, considering that in this work, the use of $(NH_4)_2Ce(NO_3)_6$ as a precursor increased the photocurrent from 286 to 398 mA cm^{-2}.

All synthesized photoanodes showed characteristics of n-type semiconductors. Among the different precursors, doping using cerium ammonium nitrate (P3) proved to be the most efficient in improving the PEC activity of $BiVO_4$ and reducing electron−hole recombination. Due to the deposition not occurring uniformly, doping with P1 and P2 decreased the photoanode PEC activity. It is worth noting that the results obtained refer to the BiOI film deposition method,[21] and there are other methods that can be used to obtain the $BiVO_4$ film. In these other cases, the results may vary between different precursors. Finally, we highlight the careful need to evaluate which rare earth dopant precursor will be used to improve the PEC activity of $BiVO_4$, considering that the same dopant may present different activity depending on the precursor used.

CONCLUSIONS

The use of different cerium precursors proved to influence the nanoscale-thick Ce−$BiVO_4$ electrochemical doping, changing the PEC properties of the obtained material. Considering the synthesis via BiOI film obtention at the nanoscale, all the films showed the presence of cerium by the physical character-

https://doi.org/10.1021/acsanm.4c03537
ACS Appl. Nano Mater. 2024, 7, 19569−19578

ization. The use of cerium(III) nitrate decreased the activity of the $BiVO_4$ film, while the use of ammonium cerium(IV) nitrate showed a better performance with a more uniform film than the pure $BiVO_4$. Therefore, it is possible to state that among the precursors used, P3 achieved a photocurrent approximately 1.4 times greater than the other precursors. Furthermore, P3 also proved to be more effective at reducing resistance to charge transfer. The reaction with H_2O_2 and HNO_3 transforms the cerium(IV) oxide precursor into cerium(III) nitrate and the results obtained were close. All of the experiments highlight the careful need to evaluate which rare earth dopant precursor will be used to improve the PEC activity of $BiVO_4$ for water splitting, considering that the same dopant may present different activity depending on the used precursor. Finally, it was demonstrated that the Ce−$BiVO_4$ anode can be efficient for application in the production of green H_2, being a promising alternative in water electrolysis.

■ ASSOCIATED CONTENT

Supporting Information

The Supporting Information is available free of charge at https://pubs.acs.org/doi/10.1021/acsanm.4c03537.

PEC characterizations including SEM images with low magnification, linear voltammograms, Nyquist EIS plots, Ce−BiOI electrodeposited charge, and photoanode stability tests (PDF)

■ AUTHOR INFORMATION

Corresponding Author

Lucia H. Mascaro − *LIEC—Interdisciplinary Laboratory of Electrochemistry and Ceramics, Federal University of São Carlos, São Paulo 13565-905, Brazil;* orcid.org/0000-0001-6908-1097; Email: lmascaro@ufscar.br

Authors

Matheus G. Guardiano − *LIEC—Interdisciplinary Laboratory of Electrochemistry and Ceramics, Federal University of São Carlos, São Paulo 13565-905, Brazil*

Lara K. Ribeiro − *LIEC—Interdisciplinary Laboratory of Electrochemistry and Ceramics, Federal University of São Carlos, São Paulo 13565-905, Brazil;* orcid.org/0000-0002-3206-7774

Isabelle M. D. Gonzaga − *LIEC—Interdisciplinary Laboratory of Electrochemistry and Ceramics, Federal University of São Carlos, São Paulo 13565-905, Brazil*

Complete contact information is available at: https://pubs.acs.org/10.1021/acsanm.4c03537

Author Contributions

The manuscript was written through contributions of all authors. All authors have given approval to the final version of the manuscript.

Funding

FAPESP (nos. 2013/0729-6, 2017/11986-5, 2023/11548-9, 2023/01415-1, and 2023/12399-7), CNPq (311769/2022-5), FINEP (01.22.0179.00), CAPES (88887.837241/2023-00), and CAPES consortium, Brazil.

Funding

The Article Processing Charge for the publication of this research was funded by the Coordination for the Improvement of Higher Education Personnel - CAPES (ROR identifier: 00x0ma614).

Notes

The authors declare no competing financial interest.

■ ACKNOWLEDGMENTS

The authors are grateful to the São Paulo State Research Foundation, Brazil, for financial support (FAPESP grant nos. 2013/07296, 2023/11548-9, 2023/01415-1, and 2023/12399-7), to the National Council for Scientific and Technological Development (CNPq grant nos. 158689/2023-2 and 311769/2022-5), and to the Coordenação de Aperfeiçoamento de Pessoal de Nível Superior (CAPES, grant no. 88887.837241/2023-00). L. H. Mascaro thanks the Financier of Studies and Projects (FINEP grant no. 01.22.0179.00), CAPES consortium, Brazil, FAPESP (2017/11986-5), Shell, and the strategic importance of the support given by ANP (Brazil's National Oil, Natural Gas, and Biofuels Agency).

■ ABBREVIATIONS

PEC, photoelectrochemical; XRD, X-ray diffraction; FE-SEM, field-emission scanning electron microscopy; SEM-EDS, scanning electron microscopy−energy-dispersive spectroscopy; VB, valence band; CB, conduction band; E_{gap}, band gap value; WE, working electrode; CV, cyclic voltammetry; LSV, linear sweep voltammetry; EIS, electrochemical impedance spectroscopy; M−S, Mott−Schottky plot; j_{pc}, photocurrent density.

■ REFERENCES

(1) Tee, S. Y.; Win, K. Y.; Teo, W. S.; Koh, L. D.; Liu, S.; Teng, C. P.; Han, M. Y. Recent Progress in Energy-Driven Water Splitting. *Adv. Sci.* **2017**, *4* (5), 1600337.

(2) Nacional, P. *European Union Announces Construction of Hydrogen Plant*.

(3) Acar, C.; Dincer, I.; Naterer, G. F. Review of Photocatalytic Water-Splitting Methods for Sustainable Hydrogen Production. *Int. J. Energy Res.* **2016**, *40* (11), 1449−1473.

(4) Joy, J.; Mathew, J.; George, S. C. Nanomaterials for Photoelectrochemical Water Splitting − Review. *Int. J. Hydrogen Energy* **2018**, *43* (10), 4804−4817.

(5) Zhang, J.; Wei, X.; Zhao, J.; Zhang, Y.; Wang, L.; Huang, J.; She, H.; Wang, Q. Electronegative Cl− Modified BiVO4 Photoanode Synergized with Nickel Hydroxide Cocatalyst for High-Performance Photoelectrochemical Water Splitting. *Chem. Eng. J.* **2023**, *454* (P1), 140081.

(6) Kim, J. H.; Lee, J. S. BiVO4-Based Heterostructured Photocatalysts for Solar Water Splitting: A Review. *Energy Environ. Focus* **2014**, *3* (4), 339−353.

(7) Liu, J.; Li, J.; Li, Y.; Guo, J.; Xu, S.-M.; Zhang, R.; Shao, M. Photoelectrochemical Water Splitting Coupled with Degradation of Organic Pollutants Enhanced by Surface and Interface Engineering of BiVO4 Photoanode. *Appl. Catal., B* **2020**, *278*, 119268.

(8) Zhao, Y.; Wang, Y.; Chi, H.; Zhang, Y.; Sun, C.; Wei, H.; Li, R. Coupling Photocatalytic Water Oxidation on Decahedron BiVO4 Crystals with Catalytic Wet Peroxide Oxidation for Removing Organic Pollution in Wastewater. *Appl. Catal., B* **2022**, *318*, 121858.

(9) Lu, X.; Ye, K.; Zhang, S.; Zhang, J.; Yang, J.; Huang, Y.; Ji, H. Amorphous Type FeOOH Modified Defective BiVO4 Photoanodes for Photoelectrochemical Water Oxidation. *Chem. Eng. J.* **2022**, *428*, 131027.

(10) Petruleviciene, M.; Savickaja, I.; Juodkazyte, J.; Grinciene, G.; Ramanavicius, A. Investigation of BiVO4-Based Advanced Oxidation System for Decomposition of Organic Compounds and Production of Reactive Sulfate Species. *Sci. Total Environ.* **2023**, *875*, 162574.

(11) Lee, Y. Y.; Sriram, B.; Wang, S. F.; Kogularasu, S.; Chang-Chien, G. P. A Comprehensive Review on Emerging Role of Rare Earth Oxides in Electrochemical Biosensors. *Microchem. J.* **2023**, *193*, 109140.

(12) Kalanoor, B. S.; Seo, H.; Kalanur, S. S. Multiple Ion Doping in BiVO4 as an Effective Strategy of Enhancing Photoelectrochemical Water Splitting: A Review. *Mater. Sci. Energy Technol.* **2021**, *4*, 317−328.
(13) Govindaraju, G. V.; Morbec, J. M.; Galli, G. A.; Choi, K.-S. Experimental and Computational Investigation of Lanthanide Ion Doping on BiVO 4 Photoanodes for Solar Water Splitting. *J. Phys. Chem. C* **2018**, *122* (34), 19416−19424.
(14) Tian, K.; Wu, L.; Han, T.; Gao, L.; Wang, P.; Chai, H.; Jin, J. Dual Modification of BiVO4 Photoanode by Rare Earth Element Neodymium Doping and Further NiFe2O4 Co-Catalyst Deposition for Efficient Photoelectrochemical Water Oxidation. *J. Alloys Compd.* **2022**, *923*, 166352.
(15) Wang, M.; Wu, L.; Zhang, F.; Gao, L.; Geng, L.; Ge, J.; Tian, K.; Chai, H.; Niu, H.; Liu, Y.; Jin, J. Doping with Rare Earth Elements and Loading Cocatalysts to Improve the Solar Water Splitting Performance of BiVO4. *Inorganics* **2023**, *11* (5), 203.
(16) Xu, H.; Wu, C.; Li, H.; Chu, J.; Sun, G.; Xu, Y.; Yan, Y. Synthesis, characterization and photocatalytic activities of rare earth-loaded BiVO4 catalysts. *Appl. Surf. Sci.* **2009**, *256* (3), 597−602.
(17) Zhang, A.; Zhang, J. Effects of Europium Doping on the Photocatalytic Behavior of BiVO4. *J. Hazard. Mater.* **2010**, *173* (1−3), 265−272.
(18) Moscow, S.; Kavinkumar, V.; Sriramkumar, M.; Jothivenkatachalam, K.; Saravanan, P.; Rajamohan, N.; Vasseghian, Y.; Rajasimman, M. Impact of Erbium (Er) and Yttrium (Y) Doping on BiVO4 Crystal Structure towards the Enhancement of Photoelectrochemical Water Splitting and Photocatalytic Performance. *Chemosphere* **2022**, *299* (December2021), 134343.
(19) Chen, X. Y.; Fang, F.; Ng, A. M. C.; Djurišić, A.; Chan, W. K.; Lui, H. F.; Fong, P. W. K.; Surya, C.; Cheah, K. W. Effect of Doping Precursors on the Optical Properties of Ce-Doped ZnO Nanorods. *Thin Solid Films* **2011**, *520* (3), 1125−1130.
(20) Kansaard, T.; Songpanit, M.; Noonuruk, R.; Wattanawikkam, C.; Mekprasart, W.; Boonyarattanakalin, K.; Jayasankar, C. K.; Pecharapa, W. Er-Doped BiVO4/BiFeO3 Nanocomposites Synthesized via Sonochemical Process and Their Piezo-Photocatalytic Application. *Nanomaterials* **2024**, *14* (11), 954.
(21) McDonald, K. J.; Choi, K. S. A New Electrochemical Synthesis Route for a BiOI Electrode and Its Conversion to a Highly Efficient Porous BiVO4 Photoanode for Solar Water Oxidation. *Energy Environ. Sci.* **2012**, *5* (9), 8553−8557.
(22) Yuan, M.; Suriyaprakash, J.; Shan, L.; Xu, H.; Li, X.; Wu, H.; Ding, G.; Shi, Z.; Dong, L.; Zhang, F. M. Carrier Confinement Activated Explicit Solvent Dynamic of CdS/BiVO4/H2O and Optimized Photocatalytic Hydrogen Evolution Performances. *J. Colloid Interface Sci.* **2024**, *658*, 571−583.
(23) Ho-Kimura, S.; Luo, W. Reinforcement of a BiVO4 Anode with an Fe2O3 Underlayer for Photoelectrochemical Water Splitting. *Sustainable Energy Fuels* **2021**, *5* (12), 3102−3114.
(24) Mane, P.; Burungale, V.; Bae, H.; Seong, C.; Heo, J.; Kang, S. H.; Ha, J.-S. Integration of Surficial Oxygen Vacancies and Interfacial Two-Dimensional NiFe-Layered Double Hydroxide Nanosheets onto Bismuth Vanadate Photoanode for Boosted Photoelectrochemical Water Splitting. *J. Power Sources* **2024**, *591*, 233832.
(25) Franco Peláez, D.; Rodríguez S, J. L.; Poznyak, T.; Martínez Gutiérrez, H.; Andraca Adame, J. A.; Lartundo Rojas, L.; Ramos Torres, C. J. Efficient Catalytic Activity of NiO and CeO 2 Films in Benzoic Acid Removal Using Ozone. *RSC Adv.* **2024**, *14* (6), 3923−3935.
(26) Luo, X. L.; Liu, C. J.; Chen, M. J.; Zhang, S. S.; Xu, Y. H. Electrochemical Performance and Enhanced Photocatalytic Activity of Ce-Doped BiVO4 under Visible Light Irradiation. *Mater. Res. Bull.* **2017**, *94*, 428−434.
(27) Jang, M. S.; Park, H. L.; Kim, J. N.; Ro, J. H.; Park, Y. H. Raman Spectrum in Monoclinic BiVO4. *Jpn. J. Appl. Phys.* **1985**, *24* (S2), 506.
(28) Ahmadi, M.; Alavi, S. M.; Larimi, A. Highly Active Platinum Decorated BiVO4 nanosheet/TiO2 Nanobelt Heterojunction for Photocatalytic CO2 Reduction. *Surf. Interfaces* **2024**, *45*, 103908.
(29) Wan, X.; Liu, G.; Wang, X.; Lu, D.; Fu, Y.; Guan, X.; Hu, C.; Rong, N.; Wang, H. Synergistic Improvement of Charge Separation and Injection on CuPc Modified BiVO4 for Efficient Solar Water Oxidation. *J. Photochem. Photobiol., A* **2024**, *451*, 115527.
(30) Yang, L.; Tang, Y.; Hu, A.; Chen, X.; Liang, K.; Zhang, L. Raman Scattering and Luminescence Study on Arrays of ZnO Doped with Tb3+. *Phys. B* **2008**, *403* (13−16), 2230−2234.
(31) Yang, X.; Dong, Z.; Sun, C. Q. Effects of Doping Concentration on Bond Length and Bond Energy Studied by Raman Shift. *Appl. Phys. Lett.* **2023**, *123* (5), 053101.
(32) Noor, M.; Sharmin, F.; Mamun, M. A.; Hasan, S.; Hakim, M.; Basith, M.; Basith, M. A. Effect of Gd and Y Co-Doping in BiVO4 Photocatalyst for Enhanced Degradation of Methylene Blue Dye. *J. Alloys Compd.* **2022**, *895*, 162639.
(33) Hussain, S.; Hussain, S.; Waleed, A.; Tavakoli, M. M.; Wang, Z.; Yang, S.; Fan, Z.; Nadeem, M. A. Fabrication of CuFe2O4/α-Fe2O3 Composite Thin Films on FTO Coated Glass and 3-D Nanospike Structures for Efficient Photoelectrochemical Water Splitting. *ACS Appl. Mater. Interfaces* **2016**, *8* (51), 35315−35322.
(34) Muche, D. N. F.; dos Santos, T. M. G.; Leite, G. P.; Melo, M. A.; Gonçalves, R. V.; Souza, F. L. Tailoring hematite/FTO Interfaces: New Horizons for Spin-Coated Hematite Photoanodes Targeting Water Splitting. *Mater. Lett.* **2019**, *254*, 218−221.
(35) Kim, J. H.; Lee, J. S. Elaborately Modified BiVO4 Photoanodes for Solar Water Splitting. *Adv. Mater.* **2019**, *31* (20), 1806938.
(36) Miao, F.; Wang, Z.; Tao, B.; Chu, J.; Chu, P. K. Composition Dependence of Structural, Optical, and Photoelectrochemical Properties of Nanocrystalline Neodymium-Doped Titania Photocatalyst. *Electrochim. Acta* **2013**, *112*, 32−36.
(37) Liu, Y.; Li, J.; Li, W.; Yang, Y.; Li, Y.; Chen, Q. Enhancement of the Photoelectrochemical Performance of WO3 Vertical Arrays Film for Solar Water Splitting by Gadolinium Doping. *J. Phys. Chem. C* **2015**, *119*, 14834−14842.
(38) Tong, M. H.; Chen, Y. X.; Lin, S. W.; Zhao, H. P.; Chen, R.; Jiang, X.; Shi, H. Y.; Zhu, M. L.; Zhou, Q. Q.; Lu, C. Z. Synchronous Electrochemical Anodization: A Novel Strategy for Preparing Cerium Doped TiO2 Nanotube Arrays toward Visible-Light PEC Water Splitting. *Electrochim. Acta* **2023**, *463*, 142793.
(39) Arora, Y.; Shah, A. P.; Battu, S.; Maliakkal, C. B.; Haram, S.; Bhattacharya, A.; Khushalani, D. Nanostructured MoS2/BiVO4 Composites for Energy Storage Applications. *Sci. Rep.* **2016**, *6*, 36294.
(40) Hu, X.; Yu, Y.; Yang, L. Electrocatalytic Activity of Ce-PbO2/C Anode for Acid Red B Reduction in Aqueous Solution. *J. Solid State Electrochem.* **2015**, *19* (6), 1599−1609.
(41) Li, H.; Zhou, L.; Wang, L.; Liu, Y.; Lei, J.; Zhang, J. In Situ Growth of TiO2 Nanocrystals on G-C3N4 for Enhanced Photocatalytic Performance. *Phys. Chem. Chem. Phys.* **2015**, *17* (26), 17406−17412.
(42) Harrington, D. A.; Van Den Driessche, P. Mechanism and Equivalent Circuits in Electrochemical Impedance Spectroscopy. *Electrochim. Acta* **2011**, *56* (23), 8005−8013.
(43) Xie, Z.; Yang, Y.; Fang, L.; Wang, Y.; Ding, X.; Yuan, G.; Liu, J. M. P. Photovoltaic, photo-impedance, and photo-capacitance effects of the flexible (111) BiFeO3 film. *Appl. Phys. Lett.* **2019**, *115*, 112902.
(44) Wei, X.; Zhang, J.; Wang, L.; Bai, Y.; Huang, J.; She, H.; Wang, Q. Super-Hydrophilic BiVO4/MgO/FeCo2O4 Charge Migration Achieves Efficient Photoelectrochemical Performance. *Chem. Eng. J.* **2024**, *482* (January), 149114.
(45) Parmar, K. P. S.; Kang, H. J.; Bist, A.; Dua, P.; Jang, J. S.; Lee, J. S. Photocatalytic and Photoelectrochemical Water Oxidation over Metal-Doped Monoclinic BiVO4 Photoanodes. *ChemSusChem* **2012**, *5* (10), 1926−1934.
(46) Baccaro, A.; Gutz, I. Fotoeletrocatálise Em Semicondutores: Dos Princípios Básicos Até Sua Conformação À Nanoescala. *Quim. Nova* **2017**, *41* (3), 326−339.

https://doi.org/10.1021/acsanm.4c03537
ACS Appl. Nano Mater. 2024, 7, 19569−19578

(47) de Araújo, M. A.; Coelho, D.; Mascaro, L. H.; Pereira, E. C. The Iron Oxyhydroxide Role in the Mediation of Charge Transfer for Water Splitting Using Bismuth Vanadate Photoanodes. *J. Solid State Electrochem.* **2018**, *22* (5), 1539−1548.
(48) Jiang, Z.; Liu, Y.; Jing, T.; Huang, B.; Zhang, X.; Qin, X.; Dai, Y.; Whangbo, M. H. Enhancing the Photocatalytic Activity of BiVO4 for Oxygen Evolution by Ce Doping: Ce3+ Ions as Hole Traps. *J. Phys. Chem. C* **2016**, *120* (4), 2058−2063.

https://doi.org/10.1021/acsanm.4c03537
ACS Appl. Nano Mater. 2024, 7, 19569−19578